

## Structure-Guided Design of Peptide-Based Trypsin Inhibitors

Mary E. McGrath,\* Paul A. Sprengeler, Bernard Hirschbein, John R. Somoza, Isabelle Lehoux, James W. Janc, Erik Gjerstad, Michael Graupe, Angeles Estiarte, Chandru Venkataramani, Yang Liu, Robb Yee, Joseph D. Ho, Michael J. Green, Chang-Sun Lee, Liang Liu, Vincent Tai, Jeffrey Spencer, David Sperandio, and Bradley A. Katz

*Celera Genomics, Inc., 180 Kimball Way, South San Francisco, California 94080*

*Received January 26, 2006; Revised Manuscript Received March 23, 2006*

**ABSTRACT:** Improved peptide-based inhibitors of human  $\beta$  trypsin were discovered using information gleaned from tripeptide library screening and structure-guided design methods, including fragment screening. Our efforts sought to improve this class of inhibitors by replacing the traditional Lys or Arg P1 element. The optimized compounds display low nanomolar potency against the mast cell target and several hundred-fold selectivity with respect to serine protease off targets. Thus, replacement of Lys/Arg at P1 in a peptide-like scaffold does not need to be accompanied by a loss in target affinity.

Trypsin is a homotetrameric serine protease produced almost exclusively by mast cells. After IgE receptors are cross-linked by ligand on the mast cell membrane, the heparin-stabilized hydrolase is released from granules, such that trypsin and other potent effectors are spilled into the surrounding tissue. In allergic asthma, the IgE response is excessive and inappropriate, with unfortunate effects on airway function. Released trypsin has been implicated in a number of activities associated with bronchoconstriction, inflammatory response, and airway tissue remodeling (1). Trypsin degrades vasoactive intestinal peptide (2) and activates bronchial contractile agents, such as bradykinin. It amplifies the response by promoting further mast cell degranulation (3) and has been shown to be a chemoattractant for inflammatory cells, such as neutrophils and eosinophils (4). Longer term remodeling effects are believed to be mediated through the purported increase in fibroblast (5) and smooth muscle growth associated with trypsin and by its activation of PAR-2 (6) and proteases (7, 8). Numerous small molecule inhibitors (9) of trypsin have been described (10–15) and many have ameliorated airway hyper-responsiveness and/or inflammatory response in asthma models that include sheep (16, 17), pig (18), mouse (19), guinea pig (20, 21), and even human (22). Thus, inhibition of trypsin offers a rational therapeutic approach for asthma. Because asthma drugs are likely to be chronically prescribed and a significant percentage of the patient population is pediatric, there is an especially high safety requirement. Thus, careful design of compounds to improve potency and selectivity of action toward the target is prudent.

Dozens of serine proteases with specificity characteristics similar to trypsin have been either characterized or are predicted in the human genome. Trypsin exhibits trypsin-like specificity, namely, a strong preference for Lys or Arg as the P1 substrate residue. Numerous X-ray structures in

trypsin and related proteases have identified the key interaction as a salt bridge between the positively charged substrate residue and Asp189, resident at the base of the deep S1 specificity pocket (23).

Peptidic inhibitors of trypsin-like serine proteases utilizing a formal positive charge at P1 are well-precedented (17). While they often yield good potency, they do not tend to display selectivity. Significant inhibition of one of the approximately sixty other human proteases featuring Asp189 could result in adverse effects. This could diminish the safety and, therefore, utility of any drug containing this moiety. With respect to new asthma drug characteristics, a novel therapy would have a great advantage if it could be dosed orally, rather than by the inhaled route. A formal charge, as exhibited by the common amidine- or guanidine-containing molecules, is not likely to achieve sufficient passive absorption in the intestine.

We endeavored to design a more drug-like replacement for the charged, nonspecific P1 residue in peptidic trypsin inhibitors using structure-guided compound design, including fragment screening in an appropriate model system.

## MATERIALS AND METHODS

The tripeptide substrate was screened as described previously (24). Details of the synthesis of the peptidic trypsin inhibitors described below are provided in the Supporting Information. Human  $\beta$ -trypsin was assayed as described in Chan et al. (25).

**Trypsin Crystallography.** Recombinant human  $\beta$ -trypsin was purchased from Promega (catalog number G563X). The protein was crystallized by the hanging drop vapor diffusion method under the formulation conditions of the manufacturer (2 mg/mL in 10 mM MES at pH 6.1 and 2 M NaCl) from a solution containing 0.1 M NaOAc at pH 4.6, 0.2 M ammonium sulfate, and 30% polyethylene glycol (PEG) 1500 (all reagents were obtained from Hampton Research). Crystallization drops were set up using various ratios of the protein solution/crystallization solution. Crystals appropriate for diffraction studies appeared in 2–5 days at room temperature.

\* To whom correspondence should be addressed. Current address: Gilead Sciences, Inc., 333 Lakeside Drive, Foster City, CA 94404. Telephone: (650) 522-1697. Fax: (650) 522-5899. E-mail: mary.mcgrath@gilead.com.

Crystals were soaked for 1–7 days in a solution comprised of 30% PEG 3350, 1.5 M NaCl, and 0.1 M NaOAc at pH 4.6, with compound concentrations ranging from 10 to 500 times the measured inhibition constant. Crystals were dipped in paraffin oil and flash-frozen in liquid nitrogen, and X-ray data were collected at the Advanced Light Source (ALS) on beamlines 5.0.1 and 5.0.2. Diffraction data were reduced using HKL2000 (26), and structures were solved using EPMR (27) for molecular replacement, with trypsin structure 1A0L used as the search model (28). XPLO2D (29) was used to generate parameter and topology files for refinement of the small molecules, and CNX (30) was used for refinement. For the ( $|F_o| - |F_c|$ ),  $\alpha_c$  omit map of Figure 7, the structure was refined to convergence without the bound ligand, followed by map calculations without the bound ligand.

**Trypsin–Fragment Crystallography.** Bovine trypsin was purchased from Worthington, and the benzamidine complex was crystallized as described (31). Benzamidine was removed by soaking crystals for several weeks in synthetic mother liquor made by saturating a solution of 1.9 M  $\text{MgSO}_4 \cdot 7\text{H}_2\text{O}$ , 1.0 mM  $\text{CaCl}_2$ , 150 mM Tris at pH 7.0 with PEG 12 000 and adjusting the pH to 7.0. Removal of benzamidine was confirmed by structure determination. After removal of benzamidine, trypsin crystals were soaked in the  $\text{MgSO}_4$ –PEG 12 000 synthetic mother liquor at saturating concentrations of fragments for at least 1 week. The synthetic mother liquor fragment soaking solutions were prepared by adding 25  $\mu\text{L}$  of a saturated dimethylsulfoxide (DMSO) solution of the fragment to 1.0 mL of the  $\text{MgSO}_4$ –PEG solution. The pH of the final soaking solution was adjusted to  $\sim 7.0$  before soaking.

X-ray diffraction data sets for trypsin–fragment complexes were collected with an R-AXIS IV<sup>++</sup> image plate, using X-rays from a Rigaku RUH3R generator operating at 50 kV and 100 mA, equipped with Osmic mirrors. The X-ray equipment and the data reduction software, Crystal Clear, were from the Molecular Structure Corporation (MSC, The Woodlands, TX). The irradiated crystals were cooled to 10 °C with a stream of nitrogen produced with a crystal cooler from Kinetics, Inc.

Structures of complexes were determined by analysis of ( $|F_o| - |F_c|$ ),  $\alpha_c$  and ( $2|F_o| - |F_c|$ ),  $\alpha_c$  maps and refined with X-PLOR (32, 33).

**Molecular Modeling.** Modeling studies were carried out using the Merck Molecular Force Field to optimize geometries and calculate energies. Maestro from Schrodinger, Inc. was used to calculate the torsional rotation barriers. Molecular properties were calculated in MOE (CCG) using their descriptors [polar surface areas (PSAs) were obtained by the 2D method of Ekins]. Overlay comparisons were performed, and figures were created with either InsightII, Quanta (Accelrys), or Pymol (Delano Scientific).

## RESULTS AND DISCUSSION

**Peptide Library Screening Results.** A tripeptide library of 5920 AMC substrates was screened to map out the selectivity determinants for the S1–S3 sites of trypsin. The library is comprised of the 20 naturally occurring amino acids at each of the P1–P3 positions with the addition of citrulline and ornithine at P1 and P2, and P3 ornithine was substituted for

cysteine (of the  $22 \times 20 \times 20 = 8800$  possible AMC substrates, 5920 could be synthesized reproducibly). We endeavored to find the amino acid preferences for each site and also hoped to discover noncharged residues at the P1 position that could, along with appropriate P2 and P3 moieties, show sufficient activity to serve as a substitute for a positively charged P1 element. Perhaps not surprisingly, only Lys- and Arg-containing P1 substrates were observed to yield good velocities. The most potent peptide was Ac-Arg-Asn-Arg-AMC [velocity ( $v$ ) = 40.4 relative fluorescence units (RFUs)/min], but in general, approximately twice as many “good” Lys-P1 substrates were identified as Arg, with the most effective being Ac-Lys-Ala-Lys-AMC ( $v$  = 33.7 RFUs/min). Choosing a value of 10 RFUs/min as a velocity cutoff resulted in 42 active Lys P1 substrates (Table 1), with a preference for Asn > Ala = Gln = Ser > Pro > Asp = Glu = Val > Thr > Arg = His = Met = Phe at P2 and Arg  $\gg$  Orn  $\gg$  Gln = Lys > Met = Thr > Gly = His = Ile = Trp = Tyr > Ala = Leu = Pro = Val at P3 (Figure 1). That same velocity cutoff afforded 22 active Arg P1 molecules (Table 1) with a preference for Ala  $\gg$  Asn = Asp = His = Ser = Val  $\gg$  Gln = Glu = Ile at P2 and Arg > Lys > Orn  $\gg$  Gln  $\gg$  Thr at P3 (Figure 1). While the preferences at each site are not identical for the two P1 elements, they do show some similar trends such as a charged moiety (e.g., Arg, Lys, and Orn) being favored at P3 and the penchant for small residues such as Ala and Ser at P2.

To discover active noncharged P1 substrates that might be useful for inhibitor design, we evaluated the non-Lys/Arg P1 tripeptides that showed the highest velocity. The first of these was methionine ( $v$  = 0.27 RFUs/min) followed by Phe ( $v$  = 0.22 RFUs/min), Asp ( $v$  = 0.19 RFUs/min), and Thr ( $v$  = 0.15 RFUs/min). The size and shape similarity of methionine to lysine might make it intriguing to speculate that these values are significant, especially because the very potent protease inhibitor ecotin (34) uses a P1 methionine to interact with a host of subsite S1 Asp-containing serine proteases. However, the fact that aspartic acid is the third most active nonpositively charged P1 suggests that these results are likely not meaningful. These results likely represent noise in the data because, as mentioned above, the S1 site of trypsin has a constituent negative charge, which would be expected to repel the acid moiety of Asp.

This conclusion is supported by the fact that there are no apparent trends in the preferences at P2 and P3 of the noncharged P1 substrates with a velocity greater than 0. In addition, there is very little spread between the velocities of the most active representatives of all of the noncharged P1 elements (0.23–0.01 RFUs/min). It was interesting to note that Orn did not show more activity as a substrate than the other noncharged residues at P1. This strongly suggests that both charge at P1 and correct alignment with S1 are critical for an efficient interaction with the enzyme.

**Initial Compound Design.** We were not surprised to see that Lys and Arg P1s are highly favored for binding to trypsin. It is noteworthy that no combination of P2 and P3 residues can even partially “rescue” a non-Lys/Arg P1 with respect to trypsin affinity. The dilemma exists that, while basic side chains appear to be required for potency, they do not adequately discriminate between the set of proteases featuring Asp at the 189 position.

Table 1: Occurrence Frequency in the Substrate Library of the P2 and P3 Amino Acids for Lys and Arg P1 Molecules that Had Velocities  $\geq 10$ 

amino acid	P2						P3					
	Lys P1			Arg P1			Lys P1			Arg P1		
	frequency (vel. $\geq 10$ FRUs/min)	frequency in library	normalized frequency	frequency (vel. $\geq 10$ FRUs/min)	frequency in library	normalized frequency	frequency (vel. $\geq 10$ FRUs/min)	frequency in library	normalized frequency	frequency (vel. $\geq 10$ FRUs/min)	frequency in library	normalized frequency
Ala	5	18	0.28	4	17	0.24	1	18	0.06	0	17	0.00
Arg	1	16	0.06	0	16	0.00	8	16	0.50	7	19	0.37
Asn	8	15	0.53	3	12	0.25	0	17	0.00	0	13	0.00
Asp	3	15	0.20	3	16	0.19	0	12	0.00	0	12	0.00
Gln	5	16	0.31	1	15	0.07	4	18	0.22	3	12	0.25
Glu	3	19	0.16	1	18	0.06	0	17	0.00	0	14	0.00
Gly	0	18	0.00	0	15	0.00	2	18	0.11	0	18	0.00
His	1	1	1.00	3	9	0.33	2	14	0.14	0	7	0.00
Ile	0	14	0.00	1	17	0.06	2	18	0.11	0	18	0.00
Leu	0	19	0.00	0	16	0.00	1	19	0.05	0	16	0.00
Lys	0	17	0.00	0	19	0.00	4	14	0.29	6	18	0.33
Met	1	15	0.07	0	12	0.00	3	18	0.17	0	14	0.00
Orn	0	16	0.00	0	18	0.00	6	15	0.40	5	19	0.26
Phe	1	19	0.05	0	18	0.00	0	18	0.00	0	14	0.00
Pro	4	17	0.24	0	11	0.00	1	17	0.06	0	17	0.00
Ser	5	15	0.33	3	12	0.25	0	3	0.00	0	3	0.00
Thr	2	16	0.13	0	3	0.00	3	11	0.27	1	14	0.07
Trp	0	15	0.00	0	15	0.00	2	19	0.11	0	14	0.07
Tyr	0	19	0.00	0	16	0.00	2	18	0.11	0	16	0.00
Val	3	15	0.20	3	16	0.19	1	15	0.07	0	16	0.00
total	42	315	0.13	22	291	0.08	42	315	0.13	22	291	0.08

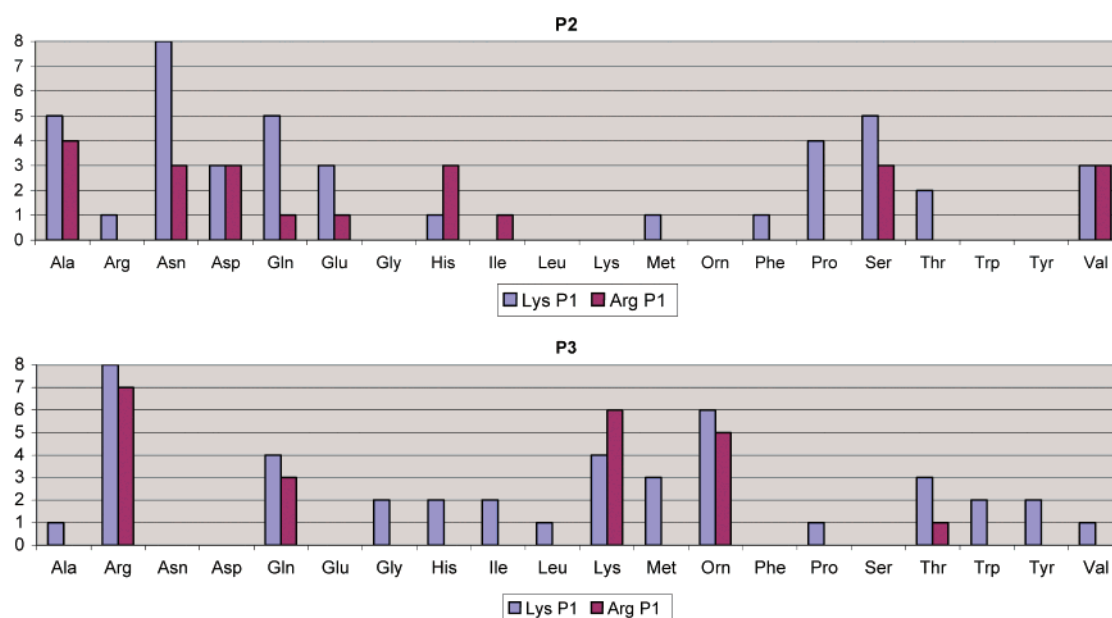


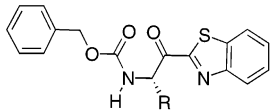

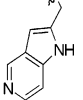

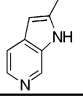
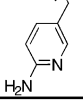
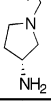
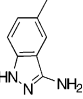
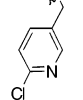
FIGURE 1: Graphical representation of the occurrence frequencies reported in Table 1.

We attempted to improve potency, selectivity, and physical properties of low-molecular-weight peptide-like inhibitors through replacement of the P1 Lys. The synthesized compounds shown in Table 2 utilize an  $\alpha$ -ketoheterocycle (35, 36) as the group targeted by the Ser195 nucleophile. The enhanced reactivity stems from the juxtaposed benzthiazole group, which withdraws electrons from the substrate ketone. As shown in Table 2, the P1 Lys compound displays a  $K_i$  value of  $7.3 \mu\text{M}$  versus trypsin and is significantly more potent against the nontarget, trypsin ( $0.69 \mu\text{M}$ ). Replacement of Lys with a variety of more drug-like fused aryl heterocycles only weakened potency. Azaindoles were tried, as well as 3-aminoindazoles and substituted pyridines. The hope was that a properly oriented aryl nitrogen could reap sufficient binding energy through the interaction with Asp189. We also

sought to reduce the number of rotatable bonds to improve the chance of intestinal absorption. However, this series of compounds underscored the challenge of finding a P1 compatible with the constraints of a peptide scaffold yet able to align productively with the carboxylate of Asp189. Subsequent modeling studies highlighted some of the challenges of successfully engaging Asp189 in the peptide context.

A small molecule, weak-binding serine protease inhibitor was used as a probe to investigate the preferred binding mode in Asp189 serine proteases. The structure of this probe, 2-aminobenzimidazole, bound to trypsin was overlaid with the structure of a typical lysine-based ketoheterocycle (also in trypsin). The structures suggest an atom for atom correspondence between the terminal four heavy atoms of

Table 2: Replacement of P1 Lys with Less Flexible and Basic Moieties

			
ID	R	Trypsin Ki (μM)	Trypsin Ki (μM)
1		7.3	0.69
2		12	6.9
3		25	2.8
4		45	13
5		>150	>150
6		>150	>150
7		>150	>150
8		>150	>150

the lysine side chain and the 1, 6, 7, and 7a atoms of 2-aminobenzimidazole (Figure 2). Models built around this design, however, indicate that there will be two negative steric interactions: one is a close contact between the carbonyl of the P3 residue and the benzene ring of the heterocycle, and the other is a disfavored torsional angle about the acyclic bond at the 6 position of the heterocycle (see Figure 3). Truncation of the designed molecule by ablation of P3 would relieve the close contact but will still suffer from the unfavorable torsion angle problem and will also lose any interaction with the protein. As shown in Table 3, molecules employing this P1 element have only a modest potency for the enzyme.

**Trypsin Crystallography.** The initial X-ray structure of trypsin had revealed that, although it is active as a noncovalent tetramer, the individual monomers bear a strong resemblance to trypsin, especially at the active site (28, 37). The unique architecture, in which all active sites face in toward a narrow central cavity, renders trypsin refractory to most proteinaceous inhibitors (38). However, the cavity is easily accessed by small molecule inhibitors of serine

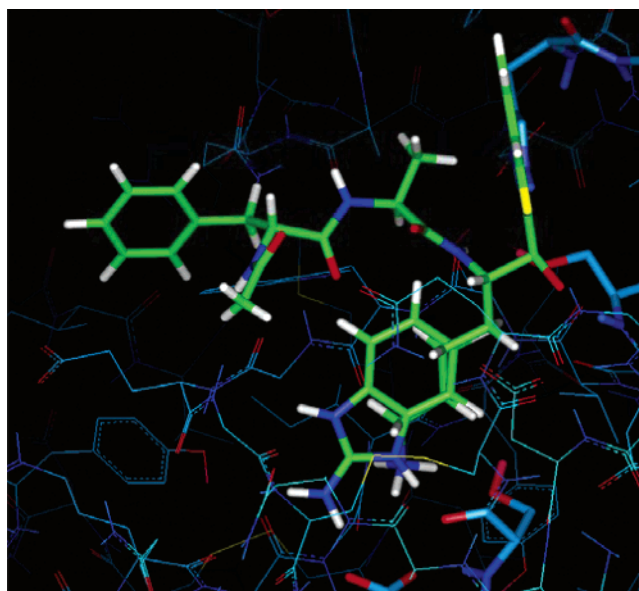


FIGURE 2: Overlay of the crystal structures of fragment 9 and ketoheterocycle CRA10.

proteases. The quaternary structure is stabilized by binding of adjacent monomers with heparin. Removal of the negatively charged proteoglycan results in conversion to the monomeric form, followed by the loss of activity (39). Because heterogeneity in heparin size can complicate trypsin crystallization efforts, we chose to crystallize human  $\beta$ 2 trypsin stabilized by high salt (2 M NaCl) rather than heparin.

**Fragment Screening Using Trypsin as a Model System.** Because the structure of 2-aminobenzimidazole provided useful information upon binding pocket specificity determinants, we sought to better understand the limitations and opportunities of the S1 pocket in trypsin by undertaking a fragment screening approach in trypsin. Figure 4a shows that a small, covalent, piperidine butyrate compound adopts similar binding modes in trypsin and trypsin. This inhibitor does not distinguish between the two similar S1 specificity pockets and highlights the appropriateness of trypsin as a model system for discovery of novel P1 moieties for trypsin. The structure of trypsin bound to the fragment 2-aminobenzimidazole was superimposed with the equivalent trypsin structure, and the comparison underscored both the promise and caveats of fragment screening. The fragment-screening approach has been used to generate new ideas for scaffolds in lead identification (Table 4). Generally, one fragment or a collection of low-molecular-weight drug-like scaffolds or fragments are soaked into crystals of the target protein. X-ray crystallography is used to visualize the binding mode (40). Binding or activity assays are generally used in conjunction with crystallography and may be used to prescreen and prioritize fragments. Affinity is generally in the high micromolar–low millimolar range for these small, nonoptimized compounds. Several companies rely on this approach as their platform technology (41, 42), and various permutations of the method have been reported. Our experience with fragment screening has highlighted its power in revealing unanticipated binding modes and its capriciousness in showing very different binding poses for closely related fragments examined in the same protein target. Thus, we use it as a more precise probe of binding pocket differences

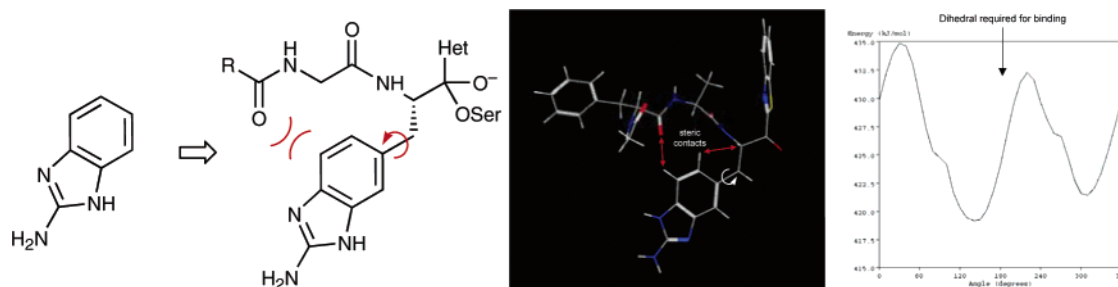


FIGURE 3: Modeling of the designed 2-aminobenzimidazole P1 element.

Table 3: Trypsin Potencies of CRA11, Fragment 9, and the P1 2-Aminobenzimidazole Compounds Designed from Them

CRA#	11	9	12	13	14
Trypsin Assay	0.023 $\mu$ M	110 $\mu$ M	18 $\mu$ M	31 $\mu$ M	94 $\mu$ M

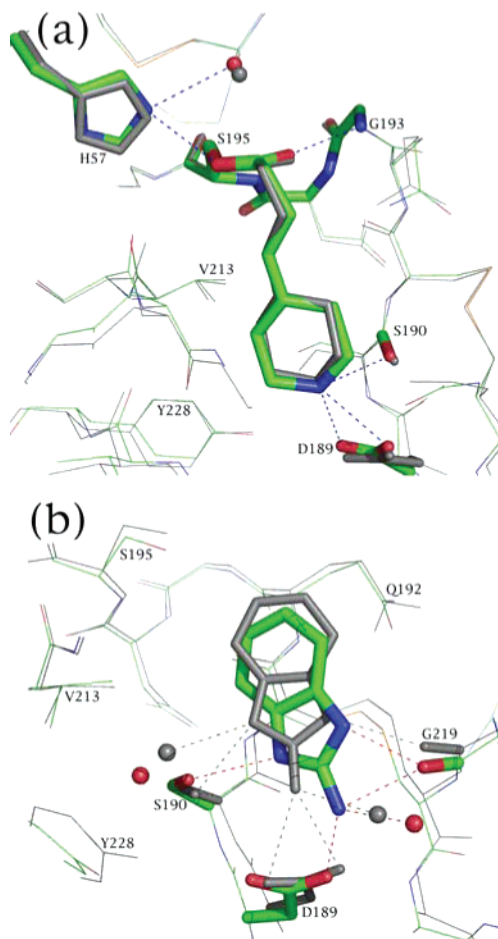


FIGURE 4: (a) Superposition of trypsin-piperidine butyrate onto tryptase-piperidine butyrate. (b) Trypsin-2-aminobenzimidazole versus the tryptase complex.

and to fully describe binding opportunities at a given site. The greater precision of the smaller molecular-weight pieces is shown in Figure 4b. Our fragment 9, 2-amino benzimidazole, is a typical representative: molecular weight < 300, reasonable balance between polar and nonpolar functional-

Table 4: Structures and  $K_i$  Values (in Millimolars) for Trypsin and Trypsin of Lead Fragments

fragment	15	9	16	17
tryptase	182	110	1800	390
trypsin	182	200	370	600
fragment	18	19	20	21
tryptase	> 2000	220	1200	220
trypsin	> 2000	560	> 2000	1000

ities (PSA = 54.7; clogP = 0.01), and drug-like in its properties. It is not constrained by bonds to any catalytic residues. It clearly displays somewhat different binding modes in tryptase and trypsin, although the larger, tethered piperidine P1 described earlier did not reveal the binding pocket idiosyncrasies. The subtle binding difference observed with 2-aminobenzimidazole alerted us to the limitations of trypsin as a model system for tryptase when using fragments. However, we acknowledge that, while fragment structure results in trypsin should not be *literally* applied to tryptase, the information gleaned from examination of a set of bound fragments can serve to reveal new binding possibilities and describe the boundaries of an Asp189-containing S1 pocket. Figure 5 shows the results of fragment-screening crystallography results in trypsin. These low-molecular-weight compounds were assayed at a high concentration versus trypsin and tryptase. The binding constants are not strictly used to prioritize fragments for subsequent crystallographic

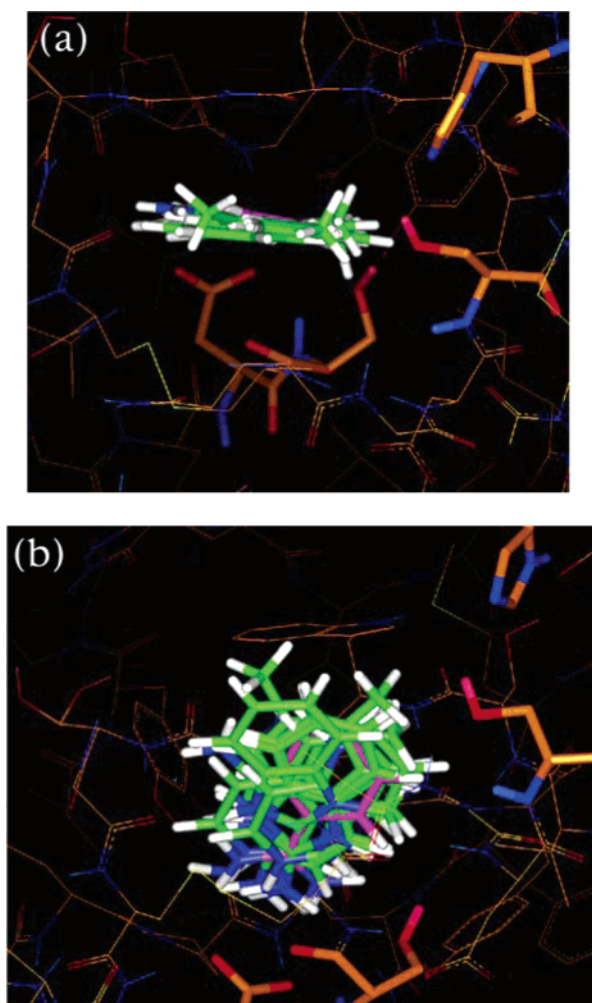
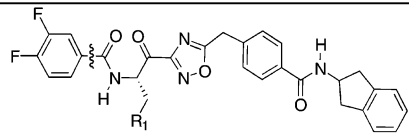


FIGURE 5: Collection of seven fragments bound in the trypsin S1 specificity pocket viewed (a) from above the catalytic triad down to Asp189 and (b) looking through the side of the S1. See also Table 6.

analysis. Rather, a set of fragments is chosen that displays a moderate affinity for the target protein, along with the diversity of structural features. Seven fragments were soaked in crystals of trypsin, and the structures were determined. In contrast to other reported protocols, fragment structures were obtained one at a time, to avoid any ambiguity as to which fragments were contributing electron density at the protease active site. The average resolution and *R* factor of these structures is 1.55 Å and 19.0%, respectively. This group of seven structures provides a striking example of the limitations and opportunities of this pocket. When the fragment set is viewed from above the S1 pocket looking directly down to its base, it appears to superimpose quite well (Figure 5a). The compounds lie in a plane that is parallel to the left side of the S1 pocket (by the standard view), specifically the strand of trypsin including residues 214–218. When the view is rotated 90°, such that the mostly planar fragments are observed perpendicular to their planes, a variety of binding modes are revealed (Figure 5b). While all fragments are bound to place their more basic end close to Asp189, the approaches differ considerably. The S1 pocket is exposed as tolerating a number of variations of binding, with fragments tilted with respect to one another and situated either more or less deeply in the pocket. The collection of structures emphasizes that Asp189 can be productively

Table 5: Optimization of P1 in a More Elaborated Scaffold

				
Corporate ID	R1	R2	Trypsin Ki (μM)	Trypsin Ki (μM)
22			0.004	0.53
23		EtO	0.003	0.17
24			0.43	74.5
25			0.025 <sup>a</sup>	1.6
26		MeO	0.13 <sup>a</sup>	5.7
27			0.006 <sup>a</sup>	0.053
28			0.021 <sup>a</sup>	7.4
29			0.59	150

<sup>a</sup> A 1:1 mixture of diastereomers at the pyrrolidine.

approached from different angles. This tolerance in the interaction with the formal negative charge is especially useful because we had seen that the vector in the S1 pocket from a peptide scaffold is far less accepting of small changes.

**Second Iteration of Compound Design.** Guided by the fragment structures in trypsin, the earlier heteroaryl compounds that did not provide potency were redesigned to relieve the unfavorable steric interactions believed to occur between peptide backbone atoms and the P1 side chain. This was accomplished by retaining two or more methylenes in P1, similar to Arg and Lys, but replacing the terminal group with a heterocycle. Several terminal groups were tested. This set of compounds is more elaborated and more potent, because improvements to the “prime side” of the molecules were occurring simultaneously with changes to P1 (Table 5). In the context of this scaffold that interacts favorably with the prime-side-binding elements on trypsin but not trypsin, a P1 Lys yields a 4 nM trypsin inhibitor. The P2 region of the molecule was also optimized, and replacement of the difluorobenzamide with an ethylcarbamate provides a 3 nM trypsin inhibitor.

A protonated lysine-based P1 element is expected to be highly hydrogen-bonded to water molecules in solution, which likely increases the desolvation energy required to pass across membranes. Inclusion of a heterocycle in the P1

Table 6: Data and Refinement Statistics

protein inhibitor data	tryptase 4-piperidinebutyrate	trypsin 4-piperidinebutyrate	trypsin 2-aminobenzimidazole	tryptase 2-aminobenzimidazole	tryptase CRA 25	tryptase CRA 23
space group	<i>P</i> 3 <sub>1</sub>	<i>P</i> 2 <sub>1</sub> 2 <sub>1</sub> 2 <sub>1</sub>	<i>P</i> 2 <sub>1</sub> 2 <sub>1</sub> 2 <sub>1</sub>	<i>P</i> 3 <sub>1</sub>	<i>P</i> 3 <sub>1</sub>	<i>P</i> 3 <sub>1</sub>
cell parameters [a, b, and c (Å)]	77.9, 77.9, 164.0	63.9, 63.2, 69.7	63.7, 63.2, 69.5	78.9, 78.9, 166.0	78.2, 78.2, 165.5	78.1, 78.1, 164.4
resolution range (Å)	20.0–2.25	38.0–1.65	29.0–1.57	20.0–2.0	50.0–2.50	20.0–2.25
number of observations	237 106	113 293	121 931	177 682	129 733	168 677
number of unique reflections	52 849	34 643	37 500	76 856	39 151	53 213
completeness (%)						
all data	99.9	99.2	99.4	98.6	99.9	100.0
highest resolution shell	100.0 (2.29–2.25 Å)	97.5 (1.74–1.65 Å)	99.1 (1.65–1.57 Å)	95.8 (2.03–2.00 Å)	98.5 (2.54–2.00 Å)	100.0 (2.29–2.25 Å)
<i>R</i> <sub>sym</sub> ( <i>I</i> ) <sup>a</sup>						
all data	0.116	0.051	0.049	0.060	0.075	0.084
highest resolution shell	0.754 (2.29–2.25 Å)	0.202 (1.74–1.65 Å)	0.270 (1.65–1.57 Å)	0.383 (2.03–2.00 Å)	0.469 (2.54–2.00 Å)	0.648 (2.29–2.25 Å)
<i>I</i> /σ( <i>I</i> )						
all data	13.1	9.3	8.8	11.6	11.5	10.0
highest resolution shell	1.9 (2.29–2.25 Å)	2.0 (1.74–1.65 Å)	1.8 (1.65–1.57 Å)	1.9 (2.03–2.00 Å)	1.6 (2.54–2.00 Å)	1.7 (2.29–2.25 Å)
model						
molecules in asymmetric unit	1 tetramer	1	1	1 tetramer	1 tetramer	1 tetramer
number of water molecules	611	157	146	520	196	292
resolution used for refinement (Å)	20.0–2.25	7.0–1.65	7.0–1.57	20.0–2.00	50.0–2.50	20.0–2.30
σ cutoff ( <i>F</i> /σ( <i>F</i> ))	0.0	0.0	0.0	0.0	0.0	0.0
<i>R</i> factor	0.202	0.190	0.203	0.208	0.204	0.212
free <i>R</i> (on the basis of ~10% of the data)	0.262	0.198	0.215	0.240	0.250	0.254
rms deviations from ideal geometry						
bonds (Å)	0.007	0.016	0.017	0.006	0.011	0.007
angles (deg)	1.45	3.50	3.70	1.37	1.55	1.41
accession code	2FWW	2FX4	2FX6	2FPZ	2FXR	2FS9

<sup>a</sup>  $R_{\text{sym}}(I) = \{\sum_{h,k,l}(I - \langle I \rangle)^2\} / \{\sum_{h,k,l} I^2\}$ .

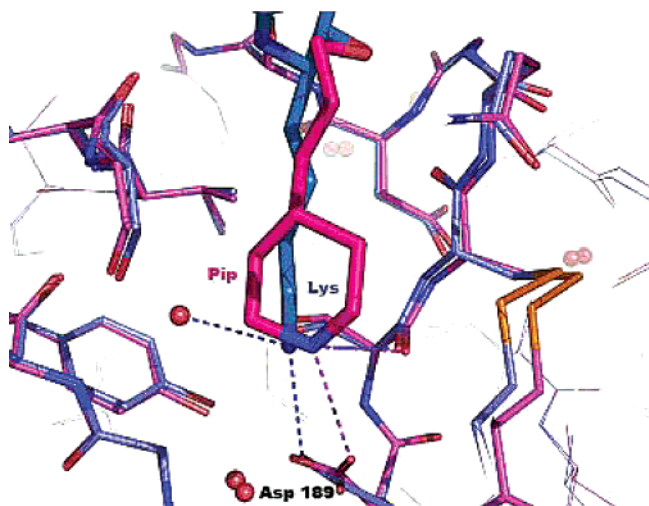


FIGURE 6: Comparison of the piperidine butyrate fragment structure with that of lysine P1 ligand, CRA 23.

element might alleviate this problem in part by removing one of these protons. Cyclization would also be expected to improve the entropy of binding by reducing the number of rotatable bonds. A comparison of the tryptase fragment structure of piperidine butyrate (Table 5) with that of a lysine P1 ligand such as CRA 23 (Figure 6) indicates that it cannot directly replace lysine because the corresponding methylene moieties are out of register even though the positively charged amine is in much the same position. The trypsin structures of a series of acyclic terminal amine-containing fragments (data not shown) suggests that this position of the positive charge is not a function of the linker because they all have similar structures. The piperidine ring does displace the S1 site water molecule, which may also improve the entropy of binding. Modeling suggests that a pyrrolidine ring, on the other hand, can be incorporated as the P1 element because it maintains the methylenes in the same register as lysine. The pyrrolidine ring would also be expected to displace the S1 site water. Attempts to obtain crystal structures of pyrrolidine-containing fragments and confirm the modeling, however, for the most part, were unsuccessful.

A pyrrolidine-containing P1, unlike the piperidine, contains an additional chiral center, which adds to the complexity of synthesis. Replacement by an azetidine removes this additional center but also shortens the overall length of the P1 element.

A P1 piperidine diminishes potency by 2 orders of magnitude, while azetidine yields an even weaker inhibitor at 590 nM. Aryl heterocycles at P1 proved unsuccessful, yielding micromolar  $K_i$  values. The related compounds with Lys at P1 all achieved nanomolar potency (data not shown). Pyrrolidine yielded potent inhibitors in the context of a number of P2 elements, with  $K_i$  values ranging from 6 to 130 nM. The arrangement of two methylenes beyond C $\alpha$ , coupled with the five-membered saturated heterocycle, clearly places the nitrogen proximal to Asp189. The X-ray crystal structure of CRA 25 bound to human tryptase indicates that this is the case.

The 2.5 Å resolution structure shows a strong density for the complete inhibitor (Figure 7). At the S1 site, the pyrrolidine nitrogen donates hydrogen bonds to one of the carboxylate oxygens of Asp189, as well as to the carbonyl of Ser190 and to a water. At the active site, there is a covalent bond between the hydroxyl of Ser195 and the activated ketone carbon of the inhibitor to make a hemiketal enzyme–inhibitor species. The other oxygen of the hemiketal occupies the oxyanion hole, accepting hydrogen bonds from the main-chain nitrogens of Gly193 and Ser195. His57 donates hydrogen bonds to the hydroxyl of Ser195 and to the nitrogen of the [1,2,4]-oxadiazole. Toward the S2 site, there is a hydrogen bond from the amide nitrogen of the inhibitor to the carbonyl of Ser214. At S1', another amide nitrogen of the inhibitor donates a hydrogen bond to the carbonyl of Cys58. The terminal indanyl group occupies the distal selectivity pocket, making hydrophobic contacts with the side chains of Val35, Phe41, Ala60, and Lys60D.

The structure of tryptase–CRA-25 can be compared with that of tryptase–CRA 23, which features a P1 Lys and the same prime side elaboration as CRA 25. [There is a small difference in the P2 moiety (allyl in CRA 25 versus methyl in CRA 23), which does not have a bearing on the P1–S1

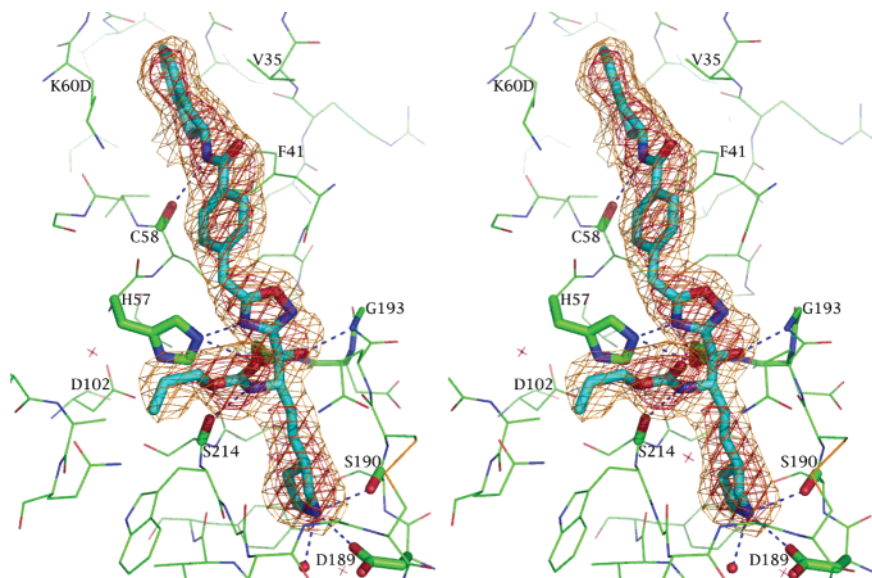


FIGURE 7: Stereoview of the refined structure of tryptase–CRA-25 (b subunit) superimposed on  $|F_o| - |F_c|$  omit map contoured at 3.0 and  $5.0\sigma$ .

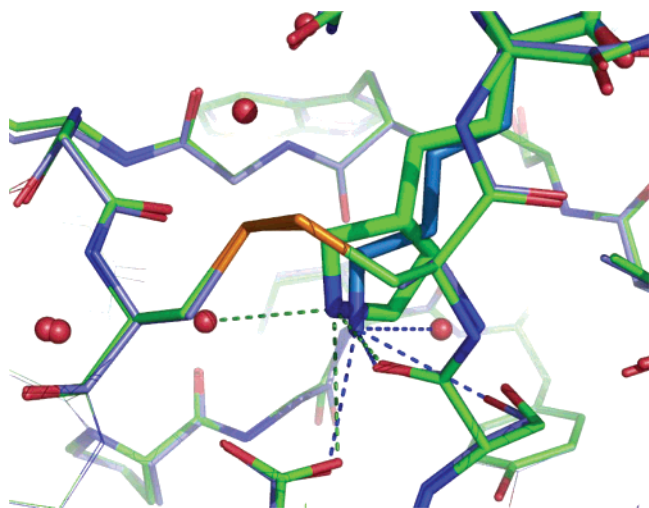


FIGURE 8: Comparison of the binding differences between the P1 elements of CRA 25 and CRA 23.

interaction, based on examination of many tryptase crystal structures (data not shown).] As expected from the earlier results, the position of the positively charged nitrogen is similar in both structures (Figure 8). In addition, the register of the methylenes is also quite similar between the two P1 elements. The pyrrolidine ring, similar to the piperidine fragment, displaces the S1 water. The additional size differences between the two P1 elements are accommodated by shifts in the position of other bound waters.

Thus, a peptidic scaffold utilizing an electron-withdrawing heterocycle and an optimized prime side group has been shown to yield potent, selective tryptase inhibitors with a more drug-like replacement for the P1 Lys.

One of the goals of this effort was to improve the oral bioavailability of the series by enhancing intestinal absorption. We had hoped that replacement of the hydrated Lys with the less solvated pyrrolidine would yield an improved compound, with respect to this parameter. Absorption by the oral route for the Lys P1 compound (CRA 22) was measured at 6% (in rats), while the P1 pyrrolidine analogue (CRA 28) was only 1.8% absorbed. The pyrrolidine compound has a slightly higher molecular weight than its Lys counterpart, with one less rotatable bond and a polar surface area of 126, compared with 140 for CRA 22. Clearly, the change in P1 has not sufficiently enhanced the oral absorption characteristics of this series. Additional design is underway to improve the oral absorption in this potent, selective scaffold.

## ACKNOWLEDGMENT

The Advanced Light Source is supported by the Director, Office of Science, Office of Basic Energy Sciences, of the U.S. Department of Energy under contract number DE-AC02-05CH11231.

## SUPPORTING INFORMATION AVAILABLE

Compound synthesis details: synthesis of 2-benzyoxycarbonylamino-3-(1H-2-(5-aza)indolyl)-4-ketobenzothiazolepropane (CRA-2) and 2-benzyoxycarbonylamino-3-(1H-2-(5-aza)indolyl)-4-ketobenzothiazolepropane (CRA-4). This material is available free of charge via the Internet at <http://pubs.acs.org>.

## REFERENCES

- Molinari, J. F., Scuri, M., Moore, W. R., Clark, J., Tanaka, R., and Abraham, W. M. (1996) Inhaled tryptase causes bronchoconstriction in sheep via histamine release, *Am. J. Respir. Crit. Care Med.* 154, 649–653.
- Tam, E. K., and Caughey, G. H. (1990) Degradation of airway neuropeptides by human lung tryptase, *Am. J. Respir. Cell Mol. Biol.* 3, 27–32.
- He, S., Gaca, M. D. A., and Walls, A. F. (1998) A role for tryptase in the activation of human mast cells: Modulation of histamine release by tryptase and inhibitors of tryptase, *J. Pharmacol. Exp. Ther.* 286, 289–297.
- He, S., Peng, Q., and Walls, A. F. (1997) Potent induction of a neutrophil and eosinophil-rich infiltrate in vivo by human mast cell tryptase: Selective enhancement of eosinophil recruitment by histamine, *J. Immunol.* 159, 6216–6225.
- Akers, I. A., Parsons, M., Hill, M. R., Hollenberg, M. D., Sanjar, S., Laurent, G. J., and McAnulty, R. J. (2000) Mast cell tryptase stimulates human lung fibroblast proliferation via protease-activated receptor-2, *Am. J. Physiol.* 278, L193–L201.
- Berger, P., Perng, D.-W., Thabrew, H., Compton, S. J., Cairns, J. A., McEuen, A. R., Marthan, R., Tunon De Lara, J.-M., and Walls, A. F. (2001) Tryptase and agonists of PAR-2 induce the proliferation of human airway smooth muscle cells, *J. Appl. Physiol.* 91, 1372–1379.
- Stack, M. S., and Johnson, D. A. (1994) Human mast cell tryptase activates single-chain urinary-type plasminogen activator (pro-urokinase), *J. Biol. Chem.* 269, 9416–9419.
- Gruber, B. L., Marchese, M. J., Suzuki, K., Schwartz, L. B., Okada, Y., Nagase, H., and Ramamurthy, N. S. (1989) Synovial procollagenase activation by human mast cell tryptase dependence upon matrix metalloproteinase 3 activation, *J. Clin. Invest.* 84, 1657–1662.
- Newhouse, B. J. (2002) Tryptase inhibitors—Review of the recent patent literature, *IDrugs* 5, 682–688.
- Levell, J., Astles, P., Eastwood, P., Cairns, J., Houille, O., Aldous, S., Merriman, G., Whiteley, B., Pribish, J., Czekaj, M., Liang, G., Maignan, S., Guilloteau, J.-P., Dupuy, A., Davidson, J., Harrison, T., Morley, A., Watson, S., Fenton, G., McCarthy, C., Romano, J., Mathew, R., Engers, D., Gardyan, M., Sides, K., Kwong, J., Tsay, J., Rebello, S., Shen, L., Wang, J., Luo, Y., Giardino, O., Lim, H.-K., Smith, K., and Pauls, H. (2005) Structure based design of 4-(3-aminomethylphenyl)piperidinyl-1-amides: Novel, potent, selective, and orally bioavailable inhibitors of b11 tryptase, *Bioorg. Med. Chem.* 13, 2859–2872.
- Combrink, K. D., Gulgeze, H. B., Meanwell, N. A., Pearce, B. C., Zulan, P., Bisacchi, G. S., Roberts, D. G., Stanley, P., and Seiler, S. M. (1998) 1,2-Benzisothiazol-3-one 1,1-dioxide inhibitors of human mast cell tryptase, *J. Med. Chem.* 41, 4854–4860.
- Zhao, G., Bolton, S. A., Kwon, C., Hartl, K. S., Seiler, S. M., Slusarchyk, W. A., Sutton, J. C., and Bisacchi, G. S. (2004) Synthesis of potent and selective 2-azepanone inhibitors of human tryptase, *Bioorg. Med. Chem. Lett.* 14, 1057.
- Murakami, Y., Takei, M., Shindo, K., Kitazume, C., Tanaka, J., Higa, T., and Fukamachi, H. (2002) Cyclotheonamide E4 and E5, new potent tryptase inhibitors from an *Ircinia* species of sponge, *J. Nat. Prod.* 65, 259–261.
- Burgess, L. E., Newhouse, B. J., Ibrahim, P., Rizzi, J., Kashem, M. A., Hartman, A., Brandhuber, B. J., Wright, C. D., Thomson, D. S., Vigers, G. P. A., and Koch, K. (1999) Potent selective nonpeptidic inhibitors of human lung tryptase, *Proc. Natl. Acad. Sci. U.S.A.* 96, 8348–8352.
- Bisacchi, G. S., Slusarchyk, W. A., Bolton, S. A., Hartl, K. S., Jacobs, G., Mathur, A., Meng, W., Ogletree, M. L., Pi, Z., Sutton, J. C., Treuner, U., Zahler, R., Zhao, G., and Seiler, S. M. (2004) Synthesis of potent and highly selective nonguanidine azetidinone inhibitors of human tryptase, *Bioorg. Med. Chem. Lett.* 14, 2227–2231.
- Clark, J. M., Abraham, W. M., Fishman, C. E., Forteza, R., Ahmed, A., Cortes, A., Warne, R. L., Moore, W. R., and Tanaka, R. D. (1995) Tryptase inhibitors block allergen-induced airway and inflammatory responses in allergic sheep, *Am. J. Respir. Crit. Care Med.* 152, 2076–2083.
- Costanzo, M. J., Yabut, S. C., Almond, H. R., Jr., Andrade-Gordon, P., Corcoran, T. W., de Garavilla, L., Kauffman, J. A., Abraham, W. M., Recacha, R., Chattopadhyay, D., and Maryanoff, B. E. (2003) Potent, small-molecule inhibitors of human mast cell

- tryptase. Antiasthmatic action of a dipeptide-based transition-state analogue containing a benzothiazole ketone, *J. Med. Chem.* **46**, 3865–3876.
18. Sylvén, H., Dahlback, M., van der Ploeg, I., and Alving, K. (2002) The tryptase inhibitor APC-366 reduces the acute airway response to allergen in pigs sensitized to *Ascaris suum*, *Clin. Exp. Allergy* **32**, 967–971.
19. Oh, S.-W., Pae, C. I., Lee, D.-K., Jones, F., Chiang, G. K. S., Kim, H.-O., Moon, S.-H., Cao, B., Ogbu, C., Jeong, K.-W., Kozu, G., Nakanishi, H., Kahn, M., Chi, E. Y., and Henderson, W. R., Jr. (2002) Tryptase inhibition blocks airway inflammation in a mouse asthma model, *J. Immunol.* **168**, 1992–2000.
20. Wright, C. D., Havill, A. M., Middleton, S. C., Kashem, M. A., Dripps, D. J., Abraham, W. M., Thomson, D. S., and Burgess, L. E. (1999) Inhibition of allergen-induced pulmonary responses by the selective tryptase inhibitor 1,5-bis-{4-[(3-carbamimidoyl-benzenesulfonylamino)-methyl]-phenoxy}-pentane (AMG-126737), *Biochem. Pharmacol.* **58**, 1989–1996.
21. Sutton, J., Bisacchi, G. S., Bolton, S. A., Hartl, K. S., Huang, M.-H., Jacobs, G., Ogletree, M. L., Pi, Z., Schumacher, W. A., Shusarchyk, W. A., Treuner, U., Zhao, G., Zahler, R., and Seiler, S. M. (2001) Synthesis and SAR of a 4-carboxy-2-azetidinone series of mechanism-based tryptase inhibitors, Abstracts of Papers, 221st ACS National Meeting, San Diego, CA, April 1–5, 2001, MEDI-249.
22. Krishna, M. T., Chauhan, A., Little, L., Sampson, K., Hawksworth, R., Mant, T., Djukanovic, R., Lee, T., and Holgate, S. (2001) Inhibition of mast cell tryptase by inhaled APC 366 attenuates allergen-induced late-phase airway obstruction in asthma, *J. Allergy Clin. Immunol.* **107**, 1039–1045.
23. Katz, B. A., Luong, C., Ho, J. D., Somoza, J. R., Gjerstad, E., Tang, J., Williams, S. R., Verner, E., Mackman, R. L., Young, W. B., Sprengeler, P. A., Chan, H., Mortara, K., Janc, J. W., and McGrath, M. E. (2004) Dissecting and designing inhibitor selectivity determinants at the S1 site using an artificial Ala190 protease (Ala190 uPA), *J. Mol. Biol.* **344**, 527–547.
24. Sheppeck, J. E., Kar, H., Gosink, L., Wheatley, J. B., Gjerstad, E., Loftus, S. M., Zubiria, A. R., and Janc, J. W. (2000) Synthesis of a statistically exhaustive fluorescent peptide substrate library for profiling protease specificity, *Bioorg. Med. Chem. Lett.* **10**, 2639–2642.
25. Yuan, J., Beltman, J., Gjerstad, E., Nguyen, M. T., Sampang, J., Chan, H., Janc, J. W., and Clark, J. M. (2006) Expression and characterization of recombinant  $\gamma$ -tryptase, *Protein Expression Purif.*, in press.
26. Otwinowski, Z., and Minor, W. (1997) in *Methods in Enzymology* (C. W. Carter, J., and Sweet, R. M., Eds.) pp 307–326, Academic Press, New York.
27. Kissenger, C. R., Gehlhaar, D. K., and Fogel, D. B. (1999) *Acta Crystallogr., Sect. D: Biol. Crystallogr.* **55**, 484–491.
28. Pereira, P. J., Bergner, A., Macedo-Ribeiro, S., Huber, R., Matschiner, G., Fritz, H., Sommerhoff, C. P., and Bode, W. (1998) Human  $\beta$ -tryptase is a ring-like tetramer with active sites facing a central pore, *Nature* **392**, 306–311.
29. Kleywegt, G. J. (1995) Dictionaries for Heteros, *CCP4/ESF-EACBM Newsletter on Protein Crystallography* **31**, 45–50.
30. Brunger, A. T., Adams, P. D., Clore, G. M., DeLano, W. L., Gros, P., Grosse-Kuntleve, R. W., Jiang, J.-S., Kuszewski, J., Nilges, M., Pannu, N. S., Read, R. J., Rice, L. M., Simonson, T., and Warren, G. L. (1998) *Acta Crystallogr., Sect. D: Biol. Crystallogr.* **54**, 905–921.
31. Katz, B. A., and Luong, C. (1999) Recruiting  $Zn^{+2}$  to mediate potent, specific inhibition of serine proteases, *J. Mol. Biol.* **292**, 669–684.
32. Brunger, A. T. (1992) The free  $R$  value: A novel statistical quantity for assessing the accuracy of crystal structures, *Nature* **355**, 472–474.
33. Brunger, A. T. (1990) *X-PLOR Manual, Version 3.1: A System for X-ray Crystallography and NMR*, pp 187–206, Yale University, New Haven, CT.
34. McGrath, M. E., Erpel, T., Bystroff, C., and Fletterick, R. J. (1994) Macromolecular chelation as an improved mechanism of protease inhibition: Structure of the ecotin–trypsin complex, *EMBO J.* **13**, 1502–1507.
35. Edwards, P. D., Wolanin, D. J., Andisik, D. W., and Davis, M. W. (1995) Peptidyl  $\alpha$ -ketoheterocyclic inhibitors of human neutrophil elastase. 2. Effect of varying the heterocyclic ring on in vitro potency, *J. Med. Chem.* **38**, 76–85.
36. Chan, A. W. E., and Golec, J. M. C. (1996) Prediction of relative potency of ketone protease inhibitors using molecular orbital theory, *Bioorg. Med. Chem.* **4**, 1673–1677.
37. Sommerhoff, C. P., Bode, W., Pereira, P. J. B., Stubbs, M. T., Sturzebecher, J., Piechotka, G. P., Matschiner, G., and Bergner, A. (1999) The structure of the human bII-tryptase tetramer: Fo-(u)r better or worse, *Proc. Natl. Acad. Sci. U.S.A.* **96**, 10984–10991.
38. Stubbs, M. T., Morenweiser, R., Sturzebecher, J., Bauer, M., Bode, W., Huber, R., Piechotka, G. P., Matschiner, G., Sommerhoff, C. P., Fritz, H., and Auerwald, E. A. (1997) The three-dimensional structure of recombinant leech-derived tryptase inhibitor in complex with trypsin. Implications for the structure of human mast cell tryptase and its inhibition, *J. Biol. Chem.* **272**, 19931–19937.
39. Selwood, T., McCaslin, D. R., and Schechter, N. M. (1998) Spontaneous inactivation of human tryptase involves conformational changes consistent with conversion of the active site to a zymogen-like structure, *Biochemistry* **37**, 13174–13183.
40. Blundell, T. L., Jhoti, H., and Abell, C. (2002) High-throughput crystallography for lead discovery in drug design, *Nat. Rev. Drug Discovery* **1**, 45–54.
41. Nienaber, V. L., Richardson, P. L., Klighofer, V., Bouska, J. J., Giranda, V. L., and Greer, J. (2000) Discovering novel ligands for macromolecules using X-ray crystallographic screening, *Nat. Biotechnol.* **18**, 1105–1108.
42. Card, G. L., Blasdel, L., England, B. P., Zhang, C., Suzuki, Y., Gillette, S., Fong, D., Ibrahim, P. N., Artis, D. R., Bollag, G., Milburn, M. V., Kim, S.-H., Schlessinger, J., and Zhang, K. Y. J. (2005) A family of phosphodiesterase inhibitors discovered by cocrystallography and scaffold-based drug design, *Nat. Biotechnol.* **23**, 201–207.

BI060173M